Slip and turbulence phenomena in journal bearings with application to implantable rotary blood pumps

Gordon Paul*, Amin Rezaienia*, Xiang Shen*, Eldad Avital*, Theodosios Korakianitis†

***School of Engineering and Materials Science, Queen Mary University of London, London, UK;**
†Parks College of Engineering, Aviation and Technology, Saint Louis University, St. Louis, MO, USA
Address correspondence and reprint requests to Prof. Theodosios Korakianitis, Parks College of Engineering, Aviation and Technology, Saint Louis University, St. Louis, MO 63103, USA. Phone: 314-977-8203, Fax: 314-977-8403 and E-mail: korakianitis@alum.mit.edu

Abstract

This paper describes an investigation into journal bearings with geometries and working fluid similar to centrifugal blood pumps. The aim is to describe the phenomena that cause these journal bearings to deviate from classical predictions. Experimental, analytical and numerical methods are used to investigate the behaviour of a range of bearings with geometries and working fluid similar to blood pumps. It was found that the clearance had a significant effect on the force-eccentricity characteristic of the bearing, with smallest and largest clearances deviating from classical predictions. Experimentally measured pressure distributions show that slip occurs when the clearance is small and that turbulence occurs with the largest clearances. The effects of these phenomena on lubricant pressure and blood compatibility are discussed.

Nomenclature

c – Clearance (m)
e – Eccentricity (m)
F – Force generated by lubricant pressure (N)
g – Correction factor
L – Journal length (m)
N – Rotational speed (rpm)
P – Pressure (Pa)
r – Journal radius (m)
U – Journal surface velocity (m/s)
z – Axial coordinate (m)
δ – Load angle (degrees)
θ – Azimuthal coordinate (degrees)
μ - Viscosity (Pa.s)

Non-dimensional

$\epsilon = e/c$ - Eccentric ratio
$C = 100*(c/r)$ – Clearance ratio
$\Lambda = L/d$ – Bearing slenderness ratio

1. Introduction

Cardiovascular disease is the leading cause of death globally, accounting for 31% or 17.3 million deaths worldwide in 2013, a number that is expected to increase to 23.6 million by 2030 [1]. Due to the shortage of heart donors compared with the huge demand, researchers have developed implantable blood pumps to make up for the shortfall. Understanding the behaviour of these pumps and their

effect on the blood that passes through them is essential to design pumps that are long lasting and safe.

The first generation of blood pumps were pneumatically driven volume displacement devices. These were effectively chambers which expanded and contracted like the native heart, such as the Thoratec PVAD [2]. It was found that these devices, with several moving parts and membranes, were too susceptible to wear for long term use [3]. The second generation of blood pumps were rotary devices which rotated on mechanical bearings [4], which were typically ceramic. These tended to last longer than their volume displacement predecessors and many of these pumps, such as the Thoratec Heartmate II, are still in use today. However, due to the mechanical contact, there is a risk of flow stagnation and thrombus formation at the bearing site, as well as problems with wear [5]. Consequently the third generation of blood pumps use entirely contactless impellers, which are suspended by hydrodynamic forces [6], passive magnetic suspension [7], active magnetic suspension [8], or combinations of these [9].

In most cases, especially in contactless centrifugal blood pumps, the contactless rotating impellers used in blood pumps have small (<1 mm) radial clearances and act as journal bearings. Examples include the Thoratec Heartmate III [10], the Cleveland Clinic IVAS [11], and Evaheart [12]. An exhaustive list of such pumps or detailed analysis of each of these is beyond the scope of this paper, however there is a clear journal bearing effect in each of these blood pumps due to the existence of rotating and stationary cylindrical faces with a small clearance. In some cases this is used as part of the suspension mechanism, in others it is considered a side effect. A comprehensive understanding of the behaviour of such bearings will aid the design of the next generation of blood pumps.

Journal bearing systems are composed of a rotating journal inside a sleeve, with a small clearance between the two filled with fluid. They allow a load to be supported without contact due to lubricant pressure generated by the journal's rotation. When the journal is in an eccentric position, the film thickness around the journal circumference is not constant. Where the fluid is pushed into a decreasing gap (nozzle) positive pressure is generated and where the fluid is pushed into an increasing gap (diffuser) negative pressure is generated. At a particular eccentric position or set of eccentric positions the force on the journal due to the lubricant pressure is equal and opposite to the applied load and the journal is in equilibrium. Such a system is useful in blood pumps because it allows partial suspension of a contactless impeller.

In most previous applications, journal bearing systems used oil filled journals, with larger geometries and a much more viscous fluid than blood. These were modelled with analytical equations describing the pressure distribution across their surfaces, which generally assume the fluid flow is laminar and use a no-slip boundary condition. Several researchers have described evidence of slip [13,14] and turbulence [15] in journal bearing systems. Since analytical solutions are used for the prediction of blood pump behaviour [24], work is required to verify assumptions in classical theory and allow behaviour prediction for journal bearings in blood pumps, with different geometries and low viscosity working fluid. This paper uses analytical, computational fluid dynamics (CFD) and experimental methods to investigate and describe the behaviour of journal bearings with various geometries and working fluid similar to that found in centrifugal rotary blood pumps.

2. Methods

Three methods are used here to analyse the behaviour of a blood-pump sized journal bearing. These are an analytical method, a CFD method and an experimental method. The journal bearing and its parameters are described in Figure 1. In this paper, the eccentricity is always in the negative Y

direction, θ = 180°, and the load angle, δ, is measured from this point. The exact physical dimensions are not disclosed here; the journal radius is fixed at a value between 12.5 – 20 mm and non-dimensional clearance ratio (C) and bearing slenderness ratio (Λ) are used to describe the bearings.

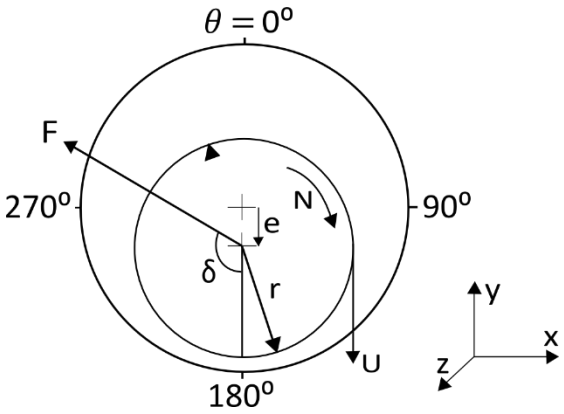

Figure 1 – A journal bearing of radius r, rotational speed N and journal surface velocity U at eccentricity e, resulting in a force F at angle δ.

In this paper the region where the film thickness is getting smaller, from 0° to 180°, is described as the nozzle region. The region where the film thickness is increasing, from 180° to 360°, is described as the diffuser region.

2.1. Analytical

An analytical method is used to predict the journal bearing load using infinitely short and infinitely long journal bearing models and correction factors proposed by Hirani et al [16]. The models for the pressure, P, at a given point on the infinitely short bearing (Ocvirk's solution P_O) [17] and the infinitely long bearing (Sommerfeld's solution, P_S) [18] are given in equations 1 and 2.

$$P_O = \frac{3\mu U L^2}{rC^2}\left[\frac{1}{4} - \left(\frac{z}{L}\right)^2\right]\frac{\epsilon.sin\theta}{(1 + \epsilon.cos\theta)^3} \quad (1)$$

$$P_S = \frac{6\mu U r}{C^2(2+\epsilon^2)}\left[\frac{\epsilon.sin\theta(2 + \epsilon.cos\theta)}{(1 + \epsilon.cos\theta)^2}\right] \quad (2)$$

Where μ is viscosity, L is journal length, r is journal radius, C is clearance ratio and ϵ is eccentricity ratio. Hirani et al demonstrate the use of correction factors g_O and g_S to combine these models to form an accurate solution for pressure at all bearing coordinates for any bearing slenderness ratio (L/2r), as described in equations 3-5.

$$\frac{1}{P} = \frac{g_O}{P_O} + \frac{g_S}{P_S} \quad (3)$$

$$g_O = 1 + \epsilon\left(\frac{L}{r}\right)^{1.2}\left[e^{\epsilon^5} - 1\right] \quad (4)$$

$$g_S = e^{(1-\epsilon)^3} \quad (5)$$

Where g is the correction factor. A Matlab code is used to calculate the pressure across the bearing according to this solution and sum it to give the force and load angle on the journal for a particular geometry, fluid, speed and eccentricity. The pressure is calculated using Hirani et al's solution for 100

radial coordinates across 20 axial coordinates for each case. A full Sommerfeld condition is applied, so the resulting load angle is always 90^{o}.

2.2. Computational fluid dynamics

Computational fluid dynamics is used to simulate the behaviour of the journal bearing in blood. Ansys mesh was used for meshing, and Ansys CFX is used as the solver. A k-ω turbulence model was used because it was considered the most appropriate to describe behaviour of the fluid in small clearances based on work by Fraser et al [19]. Ansys's documentation states that although a y^{+} value of less than 2 is desirable for a k- ω simulation, in most cases it is not achievable given the computational cost. In this study automatic near-wall treatment is used because it allows a consistent y^{+} insensitive mesh refinement from a coarser mesh. The surfaces of the journal and the sleeve are modelled as no-slip walls, and the top and bottom plane surfaces of the fluid are modelled as zero-gradient entrainment boundaries. These boundaries ensure that flow in is equal to flow out, and so the net flow across the boundary is zero. The small clearance compared to journal radius and length necessitates the use of hexahedral cells because the use of tetrahedral cells leads to an enormous number of cells.

Four divisions were used across the clearance. The number of elements varies depending on the geometry. The shortest bearing with the largest clearance has the least elements, with 26730 elements at $\epsilon = 0$ and 147246 elements at $\epsilon = 0.9$, and the longest bearing with the smallest clearance has the most elements, with 1022175 elements at $\epsilon = 0$ and 4107064 elements at $\epsilon = 0.9$. To validate the mesh density a study was carried out comparing the simulated force magnitude with a coarser and a more dense mesh than the one used. The mesh density we used gave a force magnitude 37% higher than that from a coarser mesh but only 4% lower than that with a finer mesh. We consider this error to be sufficiently small for this study. Figure 2 shows the results of the mesh study, with the y^{+} values printed by each result. Although these y^{+} values are higher than the ideal values, the automatic near-wall treatment allows a sufficiently close match with the saturated mesh at a greatly reduced computational cost, necessary given that 405 individual cases must be simulated.

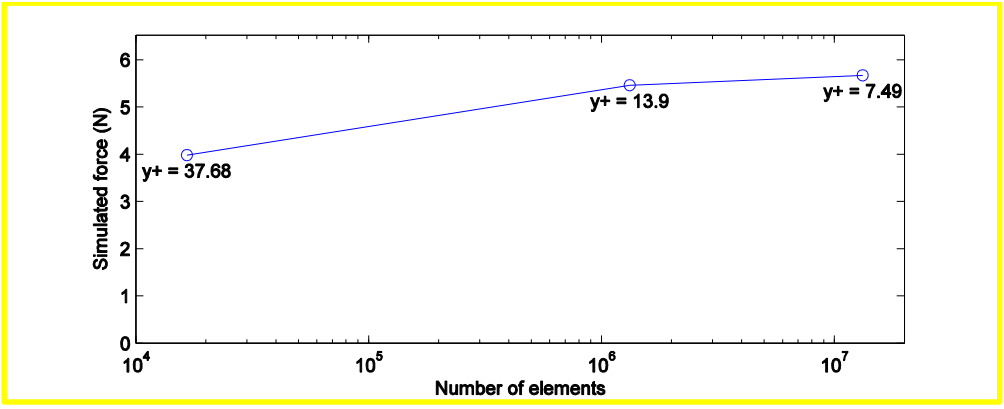

Figure 2 – A comparison of the simulated force with the mesh used in this paper, a coarser mesh and a finer mesh with C = 3.4, Λ = 0.85, ϵ = 0.9 and ω = 4000 rpm.

2.3. Experimental

A test rig was fabricated to measure the force generated by different lengths of journal bearings with different eccentricities and speeds. A journal sleeve was attached to an X-Y translation stage (Newport M-DS25-XY) to allow the sleeve to be moved to different eccentricities. This sleeve was filled with a 40% blood analogue water-glycerol solution with a density of 1.1 g/cm^3 and a viscosity of 3.6 mPa.s [20]. The X-Y translation stage is fixed to a 3 axis load cell (Interface 3AXX). The journal is fixed to the shaft of a BLDC electric motor (Maxon EC-max 60 Watt) with controllable speed. When the journal is

spinning in the journal sleeve, lubricant pressure is generated and the magnitude and direction of the resultant force on the journal sleeve can be measured from the load cell. The journal radius is varied slightly to give different clearances. The eccentric oscillation of the journal was measured and found to be below 25 µm for all journals and the casing was machined to a tolerance of +/-0.01mm. Both the load cell and the pressure sensors were calibrated before each journal bearing was tested. The test rig is shown in Figure 3.

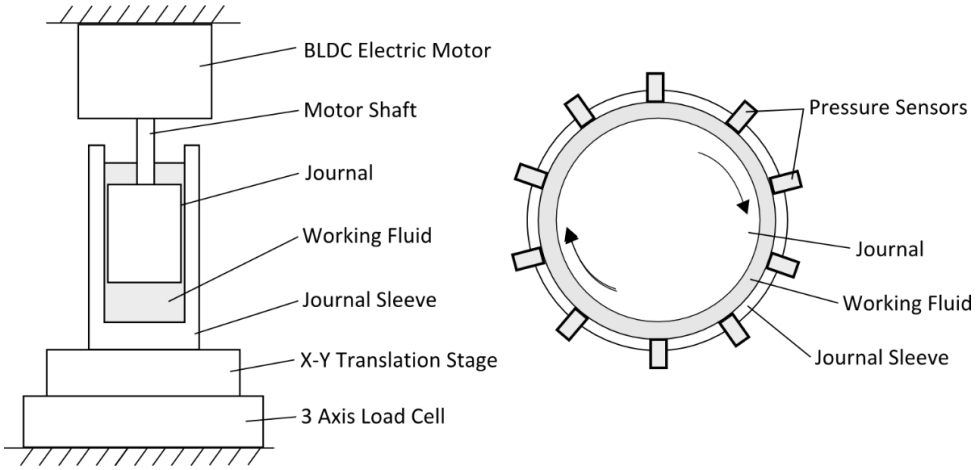

Figure 3 – Test rig to measure load magnitude and angle for small journal bearings. Left: The journal bearing test rig. Right: The pressure sensors distributed around the sleeve.

A second journal sleeve with 10 pressure sensors (Honeywell 24PCAFA6G) positioned equidistant (36^{o} spacing) around the circumference was fabricated so that the lubricant pressure distribution around the sleeve could be measured. The hole in the sleeve through which pressure was measured had a radius of 1 mm. For all pressure measurements discussed in this paper, the pressure sensors are aligned with the axial middle of the journal ($z = L/2$). Journal force and pressure distribution were measured in separate experiments so that the wires connecting the pressure sensors to external circuitry did not affect the force measured by the load cell.

3. Results

Experiments, analytical calculations and CFD simulations were performed for bearing slenderness ratios (Λ) of 0.35, 0.6 and 0.85, clearance ratios (C) of 1.7, 3.4 and 6.8, and speeds of 2000, 3000, 4000 and 5000 rpm. These values were selected to be representative of a range of blood pump designs. Eccentricities from 0.1 to 0.9 were tested in increments of 0.1. Figure 4 shows the experimentally measured force across all ϵ for all journal bearings.

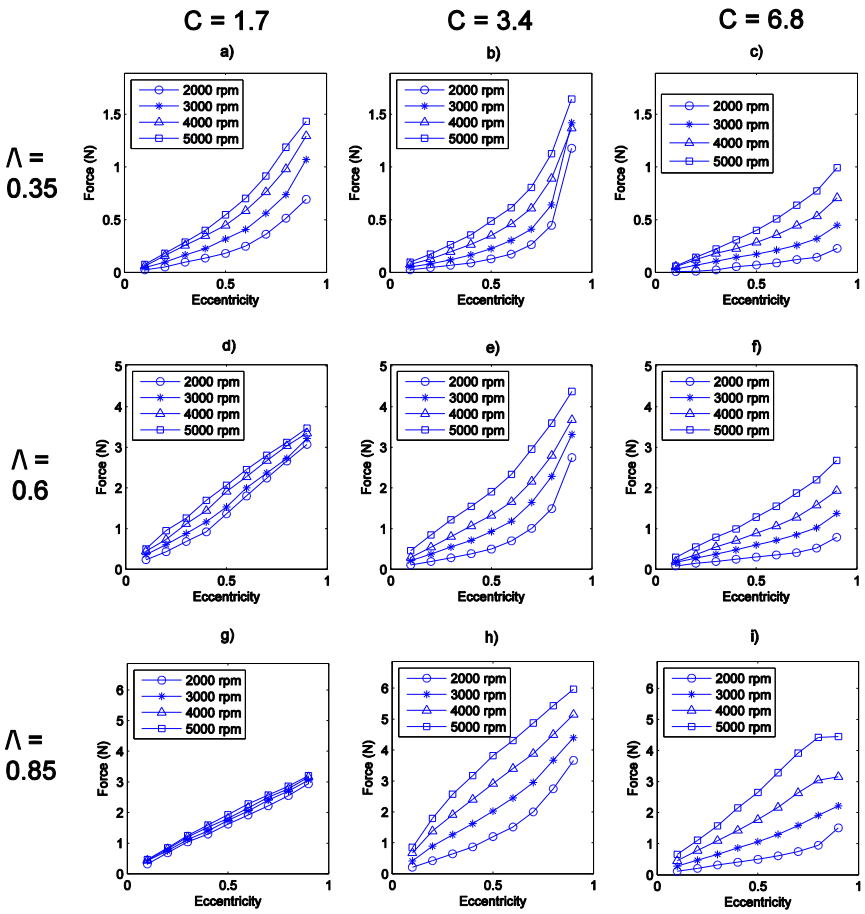

Figure 4 – Experimental results for the generated force with different journal bearings. a) C = 1.7, Λ = 0.35. b) C = 3.4, Λ = 0.35. c) C = 6.8, Λ = 0.35. d) C = 1.7, Λ = 0.6. e) C = 3.4, Λ = 0.6. f) C = 6.8, Λ = 0.6. g) C = 1.7, Λ = 0.85. h) C = 3.4, Λ = 0.85. i) C = 6.8, Λ = 0.85.

The generated force in all cases increases with increasing eccentricity. The force also increases with speed, although this effect is less pronounced as C is reduced. Shorter bearings, with a low Λ, produce a force-eccentricity characteristic closer to the classical prediction, where force increases exponentially as ϵ approaches 1. Longer bearings had a flattened curve with force approximately proportional to eccentricity.

Table 1 shows the percentage average error of generated force magnitude for analytical and CFD simulations compared to the experimental results for the three clearance ratios and three slenderness ratios. The mean error and mean absolute error for each set of data is calculated from the mean of the error for the 9 eccentricities and 4 speeds using formulae (1) and (2) respectively.

$$100\left(\sum \frac{F_{Simulation} - F_{Experimental}}{F_{Experimental}}\right) \quad (1)$$

$$100\left(\sum \frac{\left|F_{Simulation} - F_{Experimental}\right|}{F_{Experimental}}\right) \quad (2)$$

A positive mean error indicates that the simulation overestimates the experimental, while a negative mean error indicates an underestimation. The absolute mean error is given in parentheses below the mean error in the table.

Table 1 – The average error for analytical and CFD solutions compared to the experimental results. The absolute mean error is given in parentheses below the mean error. All values are given to one decimal place. * - For these large clearance (C = 6.8) simulations only ϵ = 0.1-0.5 could be solved due to vortices at ϵ = 0.6-0.9.

	Analytical			CFD		
Clearance ratio (C):	Slenderness ratio (Λ):					
	0.35	0.6	0.85	0.35	0.6	0.85
1.7	152.3% (152.3%)	122.7% (123.1%)	378.0% (378.0%)	-31.7% (50.5%)	-46.6% (57.3%)	20.3% (55.7%)
3.4	-32% (35.9%)	-21.4% (31.8%)	-4.6% (37.1%)	-4.2% (53.3%)	-1.5% (33.7%)	-7.2% (24.2%)
6.8	-46.7% (71.9%)	-59.8% (60.3%)	-49.0% (49.7%)	-28.1%* (59.3%)*	-12.7%* (27.0%)*	11.8%* (16.9%*)

At high eccentricities, the large load magnitudes predicted by the analytical model usually did not occur in the experimental. The analytical method gave an overestimation of the force in nearly every case (98.5% of cases) with the smallest clearance (C = 1.7), in some cases predicting double or triple the measured force. The same code gave an underestimation of the force in the majority of cases (94% of cases) with the largest clearance (C = 6.8). The closest match between experimental and analytical results occurred with the medium clearance (C = 3.4) where the average absolute error in predicted force was 34.9**%** of the experimental result. There was no obvious trend when comparing the analytical mean error with journal length.

The analytical simulation showed a closer match to the experimental simulation at lower speeds, with an almost exact match at 1000 rpm, while at higher speeds the characteristic of the analytical simulation deviated significantly at low and high eccentricities. The analytical and experimental results for speeds of 1000-5000 rpm with C = 3.4 and Λ = 0.85 are shown in Figure 5. As speed increases, the force at low eccentricities is underestimated and the force at high eccentricities is overestimated. The phenomena that cause the deviations at other speeds are discussed in the analysis.

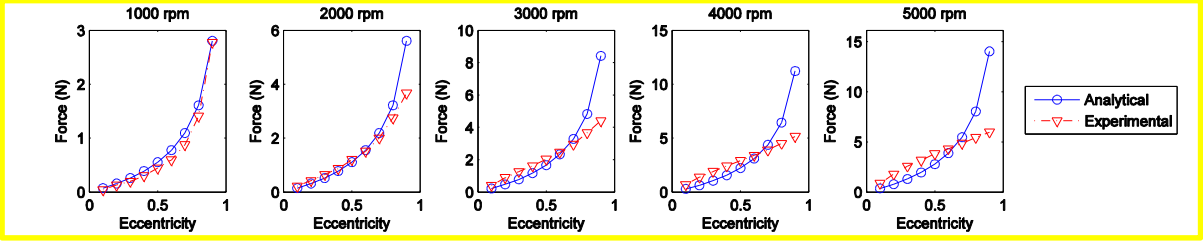

Figure 5 – Experimental and analytical results for C = 3.4, Λ = 0.85 with rotational speeds of 1000-5000 rpm.

The CFD simulation had a better agreement with the experimental results, correlating best when C = 6.8 and reasonably well with most cases with C = 3.4. However, like the analytical simulations, it was most inaccurate in predicting the behaviour of journals where C = 1.7, generally underestimating the force at low eccentricities and overestimating at high eccentricities. The CFD tended to be more accurate with longer journals. It is hypothesised that this is due to effects caused by the zero gradient entrainment openings on the top and bottom journal faces, which have a larger effect relative to a shorter journal. The CFD simulations could not be solved at C = 6.8, ϵ = 0.6-0.9 due to vortices, however the simulations that could be solved at C = 6.8 showed the closest match with the experimental, as shown in Figure 6.

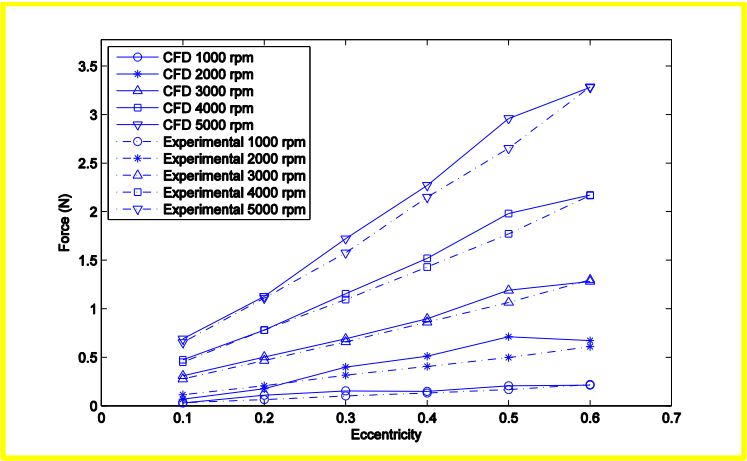

Figure 6 – Experimental and CFD results for C = 6.8, Λ = 0.85 with rotational speeds of 1000-5000 rpm.

The CFD results showed the same trends observed in the experimental results for C = 3.4 and C = 6.8 cases. The mesh density used was necessary in order to solve the large number of cases (405 individual simulations) with the available computational resources, to be able to examine the trends in the results. It is acknowledged that a denser mesh would give greater accuracy and simulation models can be tailored to specific cases for an individual analysis using processes such as a mesh-independent study, which could not be applied to each of the 405 cases in this paper.

For the simulation of C = 1.7 neither CFD nor analytical solutions were close to the experimental results, and neither result showed the lack of correlation between rotary speed and force magnitude observed in the experiment (see especially Figure 4(g)). For the simulation of C = 3.4 and C = 6.8, the analytical solution tended to be more accurate at lower speeds, while the CFD solution was more accurate at higher rotary speeds. The average absolute error for CFD and analytical simulations where C = 3.4 and C = 6.8 at different rotary speeds are described in Figure 7.

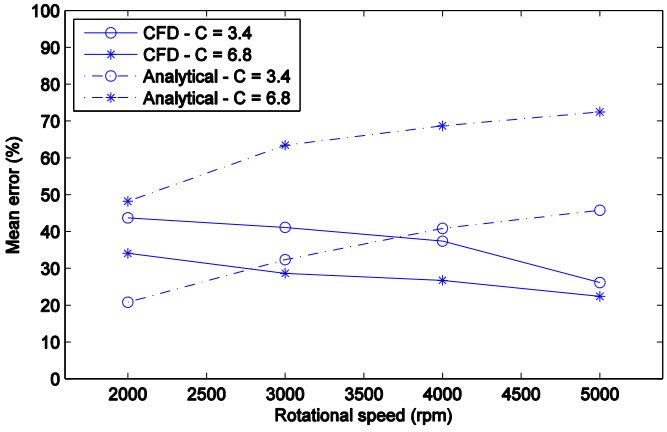

Figure 7 – Mean error for CFD and analytical solutions at various speeds.

4. Analysis

The results clearly suggest that two separate phenomena occur which cause the experimental journal bearing to deviate in behaviour from the numerical predictions. One effect dominates in cases with a small clearance, C = 1.7, and causes generated forces to be lower than predicted by the analytical model and to increase minimally with increases in rotor speed. The other dominates in cases with a large clearance, C = 6.8, and causes generated forces to be higher than predicted by the analytical

model but to be predicted correctly by the CFD simulations. In this analysis a hypothesis that the former effect is slip and the latter is turbulence is explored.

When the clearance is small, the shear stress at the walls is high because of the high velocity gradient. In this case, slip occurs at the wall because the shear stress is greater than the attachment force at the fluid-solid interface. This effect is more significant as speed increases, because higher speed increases the velocity gradient and consequently the shear stress. Slip is not modelled in the analytical or CFD simulations, so both should overestimate the force with C = 1.7. The analytical does indeed significantly overestimate the force but the CFD does not, underestimating at lower speeds and lower eccentricities. This could be due to problems with the CFD or with the experiment which are discussed in the limitations section.

When the clearance is large, turbulent flow occurs at the side opposite the minimum film, which can be thought of as increasing the viscosity of the fluid and accordingly increasing the film pressure. The CFD simulation models turbulence and consequently has a close agreement with these results. The analytical model, however, assumes laminar flow and consequently underestimates the force magnitude when significant turbulence occurs, notable in the results with a larger clearance.

4.1. Slip

Previously, researchers have reported that a no-slip condition is not appropriate for a number of different applications [13, 14]. It is clear from the examination of a long, small clearance bearing (Λ = 0.85, C = 1.7, Figure 4 (g)) that some effect is preventing the generated force from increasing with speed. However, despite there being minimal increase in force, the load angle increases as speed increases, due to a change in the lubricant pressure distribution. The measured load angle and clearance of this bearing are shown in Figure 8 and Figure 9.

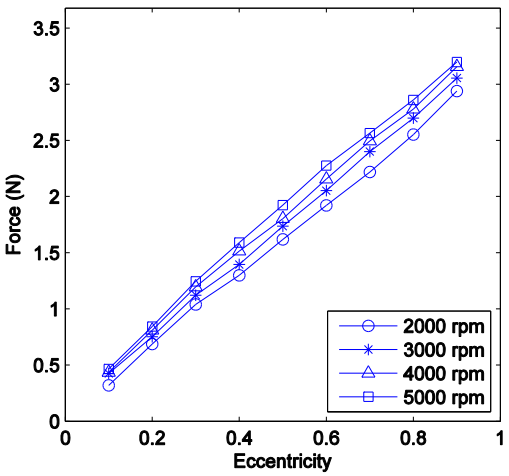

Figure 8 – Load magnitude plotted against eccentricity for a journal bearing with Λ = 0.85 and C = 1.7 at speeds from 2000 to 5000 rpm.

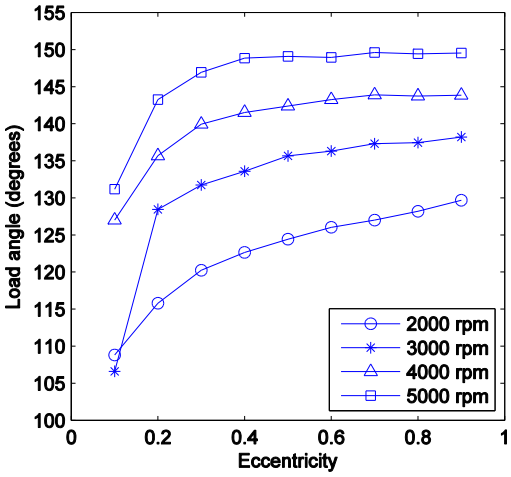

Figure 9 - Load angle plotted against eccentricity for a journal bearing with Λ = 0.85 and C = 1.7 at speeds from 2000 to 5000 rpm.

The pressure distribution around the journal was recorded using ten pressure sensors distributed around the journal sleeve. The pressure distribution of the above described journal with eccentricity 0.5 and rotational speeds of 2000, 3000, 4000 and 5000 rpm is shown in Figure 10.

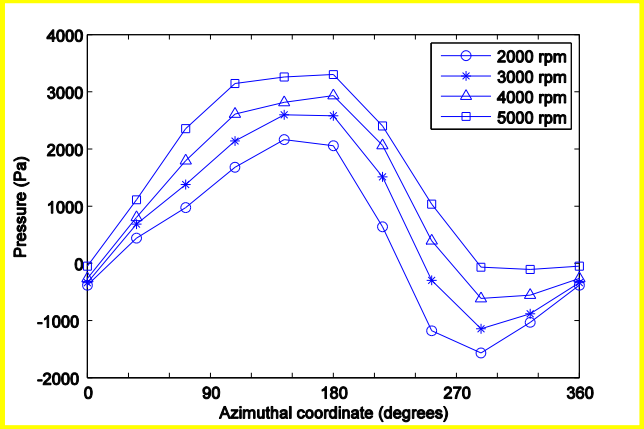

Figure 10 – Pressure distribution around the axial middle of the journal for a journal bearing with Λ = 0.85, C = 1.7 and ϵ = 0.5 at speeds from 2000 to 5000 rpm.

These results show a trend where increasing speed is associated with a reduction in the negative pressure generated. The positive pressure increases minimally with speed, whereas the classical model has P proportional to N. At higher speeds the transition to negative pressure moves further round into the diffuser zone of the journal until it is almost eradicated entirely at 5000 rpm. According to the slip model described by Ma et al [13], slip is most likely to occur where pressure is low and shear is high. It is suggested that significant slip is occurring in the diffuser region, where there is low pressure, and reducing the diffuser effect which generates negative pressure. As the speed and consequently the wall shear increases, the maximum negative pressure that can be generated falls. The maximum positive pressure is also reduced due to slip in the nozzle region.

4.2. Turbulence

In many cases with a large clearance, C = 6.8, the curve is flattened, especially notable in a longer bearing with a large clearance (Λ = 0.85, C = 6.8, Figure 4 (i)). Since this effect is prominent at large clearances, turbulence is a possible cause. Turbulence effects in journal bearings have been noted by other researchers [15]. Turbulence has the effect of increasing the generated force and reducing load angle. The force magnitude and angle for a bearing with Λ = 0.85, C = 6.8 are shown in Figure 11 and Figure 12.

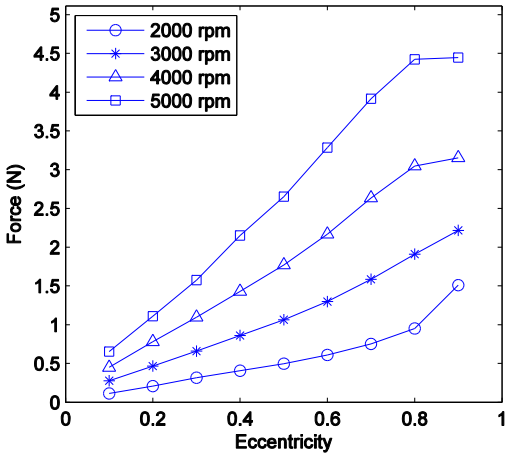

Figure 11 - Load magnitude plotted against eccentricity for a journal bearing with Λ = 0.85 and C = 6.8 at speeds from 2000 to 5000 rpm.

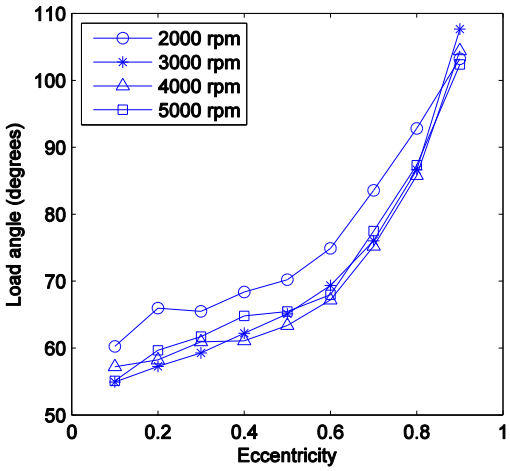

Figure 12 - Load angle plotted against eccentricity for a journal bearing with Λ = 0.85 and C = 6.8 at speeds from 2000 to 5000 rpm.

For all cases where $\epsilon<0.8$, the load angle was less than 90^o, meaning the load is actually oriented towards rather than away from the minimum film thickness. Significant turbulence occurs when the eccentricity is lower because high eccentricity limits the fluid velocity. The pressure distribution was measured for a journal bearing with $\Lambda = 0.85$, $C = 6.8$ and $\epsilon = 0.5$ at speeds from 2000 to 5000 rpm. The results are shown in Figure 13.

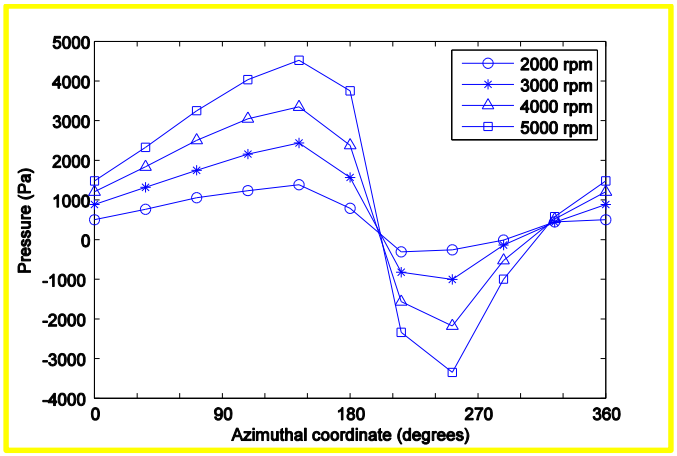

Figure 13 - Pressure distribution around the axial middle of the journal for a journal bearing with $\Lambda = 0.85$, $C = 6.8$ and $\epsilon = 0.5$ at speeds from 2000 to 5000 rpm.

These results suggest that turbulence is causing an increase in pressure all around the journal bearing, and that this extra pressure can effectively be superimposed on the classical solution to give the profiles shown in Figure 13. It was found that running a journal with $C = 6.8$ at $\epsilon = 0$ results in an increase of pressure at all pressure sensors, due to turbulence around all the journal surface. With an eccentricity, it is likely that the turbulence, and therefore the extra pressure, is greater at the maximum film thickness ($\theta = 0^o$), resulting in a force pushing towards the direction of eccentricity and a load angle of less than 90^o.

Given that there is good correlation between the CFD and experimental results at a large clearance, $C = 6.8$, CFD simulations are used to give greater understanding of this turbulence effect. By showing the eddy viscosity in the lubricant film, we can see clearly that there is an increase in effective viscosity where the film thickness is large due to turbulence. The eddy viscosity is shown on the left in Figure 14. On the right, for comparison, is a bearing with the same slenderness, speed and eccentricity and $C = 1.7$, where the eddy viscosity is far lower than the viscosity of the working fluid.

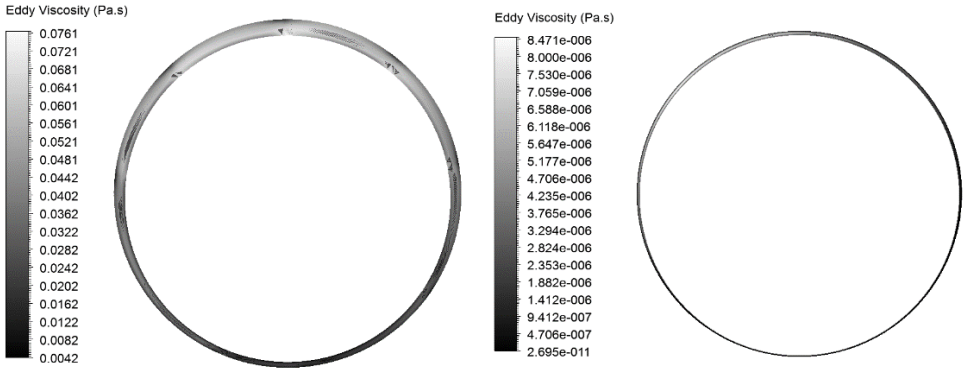

Figure 14 – Numerical solution for the eddy viscosity around the axial middle of the journal for a journal bearing with $\Lambda = 0.85$, $C = 6.8$ and $\epsilon = 0.5$ at 5000 rpm (left) and $\Lambda = 0.85$, $C = 1.7$ and $\epsilon = 0.5$ at 5000 rpm (right).

This result shows high eddy viscosity caused by turbulence around the maximum film thickness when C = 6.8, whereas eddy viscosity is several orders of magnitude lower where C = 1.7. This suggests increased pressure in the vicinity of the maximum film thickness and correlates with the experimental pressure distribution results.

4.3. Limitations

There are three main limitations to this study.

The first is that in blood pumps there is an axial pressure gradient across the radial flow paths which is not modelled here. This is difficult to implement in a controlled experiment as described here because creating a pressure gradient across the journal length requires a closed system, while measuring the force between the rotating journal and the sleeve requires that the two not be connected. The increased static pressure in a blood pump may reduce the occurrence of slip if the flow path geometry is such that high pressure exists along the radial clearance.

The second limitation is that the materials are different to those used in blood pumps. A water-glycerol blood analog solution is used instead of real blood following Boehning et al [24]. Further, the journal and sleeve are fabricated from acrylic rather than the titanium typically used in blood pumps. The attachment force at the fluid-solid interface will therefore be different in this experiment compared to the actual application. This work has nevertheless shown that slip effects can be very significant in journals with geometries, fluid density and viscosity similar to those in blood pumps. Researchers have noticed slip effects when trying to measure the viscosity of blood [21] and created models describing the slip of blood in the human body [22]. Even with a significantly stronger fluid-solid attachment, slip may occur in blood pumps which have either or a combination of a long journal length and a small radial clearance.

The third limitation is the experiment itself. Although the journals and journal sleeve were manufactured with high precision (+/-10 µm), there was a small eccentric oscillation of the journal (>25 µm) during the tests which may have affected the results by increasing turbulence. This may have affected the results, especially at a smaller clearance where the eccentric oscillation is large relative to the clearance. The effect of this is likely to be to increase turbulence and thereby increasing the experimentally measured generated force. This may explain why, where C = 1.7, the CFD simulations did not overestimate the experimentally measured force as it would be expected to due to slip. It should be noted, however, that the experimental results were highly repeatable. Initially, one journal was tested at all eccentricities three times and it was found that error was less than +/- 5% at all magnitudes, with the error most likely caused by the manual setting of eccentric displacements via a leadscrew.

4.4 Hemocompatibility

Some consideration is given here to the effects of the observed slip and turbulence phenomena on hemocompatibility in an implantable blood pump application.

When slip occurs, the load capacity falls. However, the shear stress on the blood is also decreased, reducing the chance of hemolysis. Where the pump is suspended radially by means other than a journal bearing, slip is desirable because it reduces unnecessary stress on the blood and thereby decreases blood damage in the radial clearances.

When turbulence occurs the load bearing capacity increases, however the shear stress on the blood will also increase. The vortices that are formed can increase the blood's residence time in the pump. There is evidence that vortices can have a significant impact on platelet activation [23]. Turbulence

will also increase the power consumption of a blood pump device as increased Reynolds stress increases the drag on the journal walls. This will set an upper limit on the acceptable clearance in a blood pump, depending on impeller radius and rotary speed.

5. Conclusion

This paper has shown that an analytical solution for journal bearings is only appropriate when two conditions have been met. First, there must be no slip at the journal or sleeve walls. Second, the flow must be laminar around the length of the journal. CFD simulations are more accurate than this analytical solution when turbulence occurs, although require a sophisticated method to model slip in order to give accurate results. Implementing an accurate model for wall slip between blood pump materials will form part of future work in our group.

The study in this paper aims to show these phenomena and the mechanisms behind them to improve understanding of these small journal bearing systems. In order to do this cases are shown that exemplify either slip or turbulence, however our results suggest that both effects can occur in the same bearing. The tailing off of force magnitude and increasing load angle at high eccentricities and speeds shown in a case used to exemplify turbulence (N = 4000-5000 rpm, ϵ = 0.8-0.9, Figures 11 and 12), could be slip phenomena caused by the high shear and low pressure in these conditions. CFD results can accurately model turbulence in most cases but an analytical or numerical model that can account for all these effects is outside the scope of this paper.

This paper has described some effects occurring in journal bearings with geometries and fluid viscosities similar to existing blood pumps. It was found, in agreement with Boehning et al [24], that a full Sommerfeld condition is more appropriate for modelling journal, as negative pressure is clearly generated in the diffuser region. The information provided in this paper describes situations in which slip and turbulence phenomena can occur, and what effect this has on the generated force and load angle. This improves understanding of journal bearing systems in blood pumps and hopefully informs engineers for future blood pump designs.

Acknowledgements

This report is independent research funded by the National Institute for Health Research [Investment for innovation (i4i), Turbocardia, II-LB-1111-20007]. Principal Investigator for the grant is Prof. T. Korakianitis. The views expressed in this publication are those of the authors and not necessarily those of the NHS, the National Institute for Health Research or the Department of Health.

References

[1] – Heart disease and stroke statistics – 2015 update. Circulation, 131, pp 29-322, 2015.
[2] - A versatile intracorporeal ventricular assist device based on the Thoratec VAD system, Reichenbach, Steven H and Farrar, David J and Hill, J Donald, The Annals of thoracic surgery, 71(3), pp. 171—175, 2001.
[3] - The History of Continuous-Flow Blood Pumps, Olsen, Don B, Artificial Organs, 24(6), pp. 401—404, 2000.
[4] - Optimization of Centrifugal Pump Characteristic Dimensions for Mechanical Circulatory Support Devices, Korakianitis T,Rezaienia MA, Paul GM, Rahideh A, Rothman MT, and Mozafari S. Pre-print in ASAIO journal, 2016.
[5] - Continuous-flow rotary left ventricular assist devices with "3rd generation" design, Pagani, Francis D, Seminars in thoracic and cardiovascular surgery 20(3), pp. 255—263, 2008.
[6] - VentrAssist hydrodynamically suspended, open, centrifugal blood pump, Watterson PA, Woodard JC, Ramsden VS, Reizes JA, Artificial Organs, 24(6), pp. 475-7, 2000.
[7] - Off-pump implantation of the HeartWare HVAD left ventricular assist device through minimally invasive incisions, Cheung, Anson and Lamarche, Yoan and Kaan, Annemarie and Munt, Bradley and Doyle, Aaron and Bashir, Jamil and Janz, Paul, The Annals of thoracic surgery, 91(4), pp. 1294—1296, 2011.
[8] - The effects of ambulatory accelerations on the stability of a magnetically suspended impeller for an implantable blood pump, Paul G, Rezaienia MA, Rahideh A, Munjiza A, Korakianitis T, Pre-print in Artificial Organs, 2016.
[9] - Third-generation continuous flow left ventricular assist devices, Nguyen, Duc Q and Thourani, Vinod H,
Innovations: Technology and Techniques in Cardiothoracic and Vascular Surgery, 5(4), pp. 250—258, 2010.
[10] - HeartMate III: pump design for a centrifugal LVAD with a magnetically levitated rotor, Bourque, Kevin and Gernes, David B and Loree, Howard M and Richardson, J Scott and Poirier, Victor L and Barletta, Natale and Fleischli, Andreas and Foiera, Giampiero and Gempp, Thomas M and Schoeb, Reto Litwak, Kenneth N., Akimoto, Takehide Watach, Mary J., and; Litwak, Philip, ASAIO journal, 47(4), pp. 401—405, 2001.
[11] - Stable blood lubricated hydrodynamic journal bearing with magnetic loading, Malanoski, Stanley B and Belawski, Helen and Horvath, David and Smith, William A and Golding, Leonard R, ASAIO journal, 44(5), pp. 737—740, 1998.
[12] - EVAHEART™: An implantable centrifugal blood pump for long-term circulatory support, Yamazaki, Kenji and Kihara, Shinichiro and Akimoto, Takehide and Tagusari, Osamu and Kawai, Akihiko and Umezu, Mitsuo and Tomioka, Jun and Kormos, Robert L and Griffith, Bartley P and Kurosawa, Hiromi, The Japanese Journal of Thoracic and Cardiovascular Surgery, 50(11), pp. 461—465, 2002.
[13] - Abnormal behavior of a hydrodynamic lubrication journal bearing caused by wall slip, Wu, CW and Ma, GJ, Tribology international, 38(5), pp. 492—499, 2005.
[14] - Numerical prediction of slip flow effect on gas-lubricated journal bearings for MEMS/MST-based micro-rotating machinery, Lee, Yong-Bok and Kwak, Hyun-Duck and Kim, Chang-Ho and Lee, Nam-Soo, Tribology international, 38(2), pp. 89—96, 2005.
[15] - Study on mixing flow effects in a high-speed journal bearing, Chun, Sang Myung and Ha, Dae-Hong, Tribology International, 34(6), pp. 397—405, 2001.
[16] - Rapid performance evaluation of journal bearings, Hirani, H and Rao, TVVLN and Athre, K and Biswas, S, Tribology international, 30(11), pp. 825—834, 1997.
[17] - Short-bearing approximation for full journal bearings, F.W. Ocvirk, NACA Technical Note 2808, 1952.
[18] - The hydrodynamic theory of lubrication friction, Sommerfeld, A, Z. Math. Phys, 50(1-2), pp. 97—155, 1904.
[19] - The use of computational fluid dynamics in the development of ventricular assist devices, Fraser, KH and Taskin, ME and Griffith, BP, Wu, ZJ, Medical engineering & physics, 33(3), pp. 263—280, 2011.
[20] - Segur JB, Oberstar HE, Viscosity of glycerol and its aqueous solutions, Industrial & Engineering Chemistry, 43(9), pp. 2117-20, 1951.
[21] - Blood flow, slip, and viscometry, Nubar, Yves, Biophysical journal, 11(3), pp. 252, 1971.
[22] - Blood flow through an artery with mild stenosis: a two-layered model, different shapes of stenoses and slip velocity at the wall, Ponalagusamy, R, Journal of Applied Sciences, 7(7), pp. 1071--1077}, 2007.
[23] - The use of computational fluid dynamics in the development of ventricular assist devices, Fraser, Katharine H and Taskin, M Ertan and Griffith, Bartley P and Wu, Zhongjun J, Medical engineering & physics, 33(3), pp. 263—280, 2011.
[24] - Experimental and analytical performance evaluation of short circular hydrodynamic journal bearings used in rotary blood pumps, Boehning, Fiete and Timms, Daniel and Hsu, Po-Lin and Schmitz-Rode, Thomas and Steinseifer, Ulrich, Artificial organs, 37(10), pp. 913—920, 2013.